molecules

MDPI

*Article*

# The Reactive Sites of Methane Activation: A Comparison of $IrC_3^+$ with $PtC_3^+$

**Zizhuang Liu [1], Hechen Wu [1], Wei Li [2] and Xiaonan Wu [1,*]**

[1] Department of Chemistry, Fudan University, Shanghai 200433, China; 18210220047@fudan.edu.cn (Z.L.); hcwu19@fudan.edu.cn (H.W.)
[2] School of Mathematics and Physics, North China Electric Power University, Beinong Road 2, Huilongguan, Beijing 102206, China; weil@ncepu.edu.cn
* Correspondence: wuxiaonan@fudan.edu.cn

**Abstract:** The activation reactions of methane mediated by metal carbide ions $MC_3^+$ ($M$ = Ir and Pt) were comparatively studied at room temperature using the techniques of mass spectrometry in conjunction with theoretical calculations. $MC_3^+$ ($M$ = Ir and Pt) ions reacted with $CH_4$ at room temperature forming $MC_2H_2^+/C_2H_2$ and $MC_4H_2^+/H_2$ as the major products for both systems. Besides that, $PtC_3^+$ could abstract a hydrogen atom from $CH_4$ to generate $PtC_3H^+/CH_3$, while $IrC_3^+$ could not. Quantum chemical calculations showed that the $MC_3^+$ ($M$ = Ir and Pt) ions have a linear M-C-C-C structure. The first C–H activation took place on the Ir atom for $IrC_3^+$. The terminal carbon atom was the reactive site for the first C–H bond activation of $PtC_3^+$, which was beneficial to generate $PtC_3H^+/CH_3$. The orbitals of the different metal influence the selection of the reactive sites for methane activation, which results in the different reaction channels. This study investigates the molecular-level mechanisms of the reactive sites of methane activation.

**Keywords:** mthane activation; mass spectrometry; quantum chemical calculation; ractive site



**Citation:** Liu, Z.; Wu, H.; Li, W.; Wu, X. The Reactive Sites of Methane Activation: A Comparison of $IrC_3^+$ with $PtC_3^+$. *Molecules* **2021**, *26*, 6028. https://doi.org/10.3390/molecules26196028

Academic Editors: Gang Feng and Weixing Li

Received: 13 September 2021
Accepted: 20 September 2021
Published: 4 October 2021



## 1. Introduction

Methane has attracted attention as the main component of natural gas and the conversion of methane into value-added chemicals is very important [1,2]. However, methane is extremely stable, with high C–H bond strengths (439 kJ/mol), negligible electron affinity and low polarizability [3]. At present, most of the catalytic conversion of methane needs to be carried out under high-temperature or high-pressure conditions [4]. Metal carbides are a kind of molecules with the potential to activate methane and have been studied by several groups [5]. Research on the mechanisms of the activation of methane by metal carbides is of great value and it may be helpful to find new catalysts of metal carbides [6,7]. At the same time, it is very difficult to study the activation mechanisms of methane. In recent years, people have found that the study of the gas-phase reaction of methane is an important means to study related reaction mechanisms [8,9].

Past studies have shown that gas-phase clusters are an ideal model for studying the reaction mechanisms in condensed-phase systems. The study of gas-phase clusters can reveal the specific reaction mechanisms, including the active sites, and provide references for condensed-phase catalytical processes [10]. At present, researchers are concerned about the reactions of methane with metal ions such as $Os^+$ [11], $Pt^+$ [12], $Ta^+$ [13] and Rh(0) [14] and metal oxides such as $MgO^+$ [15], $PbO^+$ [16], $V_4O_{10}^+$ [17] and $Re_2O_7^+$ [18]. In addition to metal ions and their oxides, studies have shown that metal carbides can also activate methane, such as $FeC_6^-$ [19], $Mo_2C_2^-$ [20], $Ta_2C_4^-$ [21], $FeC_3^-$ [6], $AuC^+$ [22], $FeC_4^+$ [23] and $MC^+$ [7]. These studies have explored some possible mechanisms for the activation of methane by metal carbide clusters. For example, the study of $AuC^+$ reveals a special hydride-transfer mechanism (HT) [22], while the study of $FeC_3^-$ shows that methane and atomic clusters generate CC-coupling reaction products at high temperatures and explained

the possible mechanism of non-oxidized methane aromatization at the molecular level [6]. The study of $FeC_4^+$ shows that the cluster can activate the C–H bonds of methane via the hydrogen-atom transfer (HAT) mechanism at ambient temperature; the study used the frontier orbital theory to explain the root cause of the HAT reaction [23]. Although there have been some studies on the mechanisms of metal carbides to activate methane in the past, there is still no clear investigation on the reactive sites of methane activation. Therefore, further research is needed to study the reactive sites for the activation of methane. Here, we reported the reactions of $MC_3^+$ ($M$ = Pt and Ir) with methane.

## 2. Experimental and Computational Methods

The experiments were performed using an ion trap mass spectrometer equipped with a laser vaporization–supersonic expansion ion source that was reported previously [24,25]. The $MC_3^+$ ($M$ = Pt and Ir) ions were generated by pulsed laser ablation of a rotating and translating metal/carbon (metal:carbon = 1:4) target. The nascent ablated plasma was entrained by a helium carrier gas with a backing pressure of about 0.5 MPa. The ions were mass-selected by a quadrupole and then were sent into a linear ion trap, where the ions were accumulated and cooled by helium gas. The $MC_3^+$ ions reacted with $CH_4$, $CD_4$ and $^{13}CH_4$, introduced by a pulsed valve. After a 10 ms reaction, the trapped ions were ejected for mass detection.

Theoretical calculations were performed using the Gaussian 09 package [26]. All of the calculations were performed using the BMK functional with the def2-TZVP basis sets [27,28]. Vibrational frequency calculations were employed to identify the nature of reaction intermediates, transition states (TSs) and products. The Molclus program [29] was used to search for the possible stable structures of the $MC_3^+$, $MC_2H_2^+$, $MC_4H_2^+$ and $MC_3H^+$ ($M$ = Pt and Ir). The low-lying stable isomers were then re-optimized at the BMK/def2TZVP level to confirm the relative energy sequence. Transition-state optimizations were performed with the synchronous transit-guided quasi-Newton (STQN) method and were verified through intrinsic reaction coordinate (IRC) calculations [30,31]. Vibrational frequency calculations were performed to identify the nature of reaction intermediates, transition states (TSs) and products.

## 3. Results and Discussion

The mass spectra for the reactions of mass-selected $MC_3^+$ ($M$ = Pt and Ir) ions with He (a1 and a2), $CH_4$ (b1 and b2), $CD_4$ (c1 and c2) and $^{13}CH_4$ (d1 and d2) in the ion trap at room temperature are shown in Figure 1. No product ion was observed in the mass spectra when using pure He as reactant gas, while two main peaks, at $m/z$ = 219 and 243 for the Ir-system, and $m/z$ = 222 and 246 for the Pt-system for the reactions with $CH_4$, which can be attributed to the product ions with chemical formulas $MC_2H_2^+$ and $MC_4H_2^+$ ($M$ = $^{196}$Pt and $^{193}$Ir), were observed to be the major reaction products. A weak mass peak at $m/z$ = 233 assigned to the ion with chemical formula $PtC_3H^+$ for $PtC_3^+/CH_4$ was also observed, while no $IrC_3H^+$ was found. The mass spectra suggest that two main reaction channels for both systems and one hydrogen-atom abstraction channel for $PtC_3^+$ were observed. The first channel is the formation of the $MC_2H_2^+$ cation with the release of a neutral $C_2H_2$ (reaction 1). The second channel is the generation of the $MC_4H_2^+$ ion with concomitant elimination of a dihydrogen molecule (reaction 2). The third channel is the generation of the $PtC_3H^+$ ion with the release of $CH_3$ as shown in reaction 3.

$$MC_3^+ + CH_4 \rightarrow MC_2H_2^+ + C_2H_2 \quad (1)$$

$$MC_3^+ + CH_4 \rightarrow MC_4H_2^+ + H_2 \quad (2)$$

$$PtC_3^+ + CH_4 \rightarrow PtC_3H^+ + CH_3 \quad (3)$$

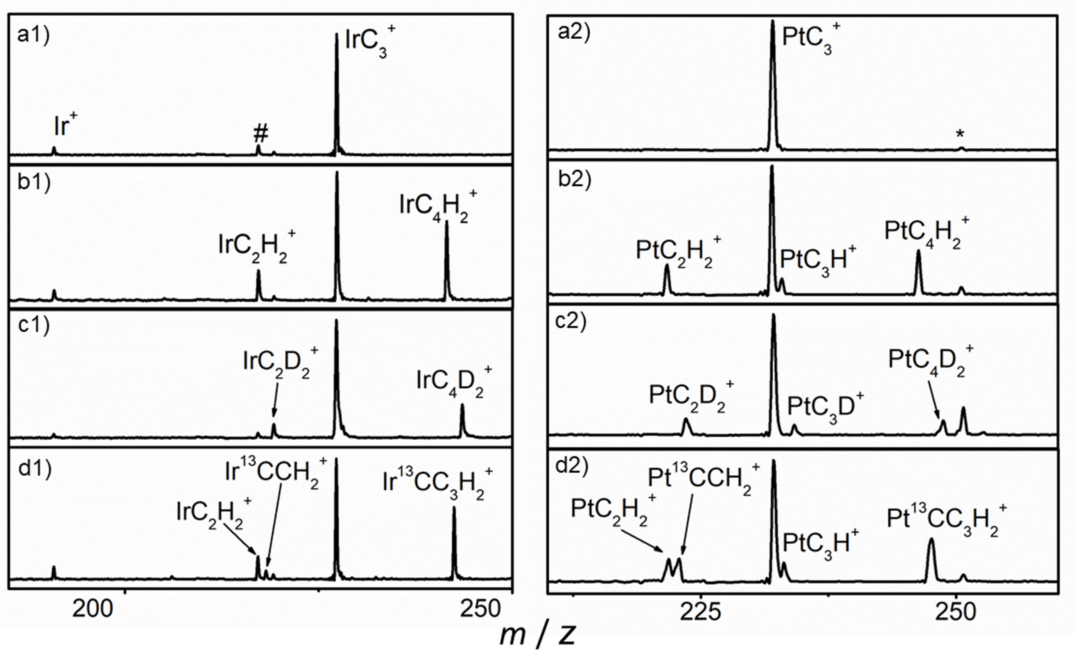


**Figure 1.** Mass spectra from the reactions of $MC_3^+$ ($M$ = Pt and Ir) with He (**a1**,**a2**), $CH_4$ (**b1**,**b2**), $CD_4$ (**c1**,**c2**) and $^{13}CH_4$ (**d1**,**d2**). # and * denote $IrCO^+$ and $PtC_3H_2O^+$.

Impurity $PtC_3{\bullet}H_2O^+$ and $IrCO^+$ ions were formed due to the small amount of contaminant in the chamber of the instrument. Isotopic-labeling experiments conducted using the $CD_4$ sample showed that there were peaks of $IrC_2D_2^+$, $IrC_4D_2^+$, $PtC_2D_2^+$, $PtC_4D_2^+$ and $PtC_3D^+$, which demonstrates that the H atoms in the products were all from methane. Both the $PtC_2H_2^+$ and $Pt^{13}CCH_2^+$ product ions were observed to have approximately the same intensity, when using $^{13}CH_4$, indicating that one or both carbon atoms of the eliminated $C_2H_2$ neutral molecule came from the $PtC_3^+$ ion. The intensity of the peak of $Ir^{13}CCH_2^+$ is similar with that of $IrC_2H_2^+$, which eliminates the background peak. The peaks of $Ir^{13}CC_3H_2^+$ and $Pt^{13}CC_3H_2^+$ were observed, which confirms the reaction channels.

In order to gain insight into the reaction mechanisms, the various possible structures of the products $MC_3^+$ ($M$ = Pt and Ir) were obtained by calculations at the BMK/def2-TZVP level and are shown in Figure S1. The most stable structures of $MC_3^+$ ($M$ = Pt and Ir) have a linear structure $M$-C-C-C, with the ground state $^1\Sigma^+$ ($IrC_3^+$) and $^2\Sigma^-$ ($PtC_3^+$). For the products (Figure S2), the most stable structures of $MC_2H_2^+$ and $MC_4H_2^+$ ($M$ = Pt and Ir) are metal cations with $C_2H_2$ and linear H-C-C-C-C-H, respectively. For $MC_3H^+$ ($M$ = Pt and Ir), the most stable structures of $MC_3H^+$ ($M$ = Pt and Ir) have a linear structure $M$-C-C-C-H, given in Figure S2.

In order to gain insight into the reaction mechanism, the potential energy profiles (PESs) were calculated. All of the three Reactions (1)–(3) leading to the stable structures of the products were exothermic. The pathways for the $IrC_3^+ + CH_4$ reaction leading to the $IrC_2H_2^+/C_2H_2$ and $IrC_4H_2^+/H_2$ products are shown in Figure 2 and details are given in Figures S3–S4. An encounter complex ($^3I1$), that is −1.51 eV lower in energy than the ground state reactants, is formed initially. The Ir atom serves as the active site of the reaction and intermediate $^1I2$ is formed via the first C–H bond activation. Then, the $CH_3$ moiety is transferred to $C_3$ to form a C–C bond; meanwhile, one H atom is transferred to the Ir atom ($^1I2 \rightarrow {}^1TS2 \rightarrow {}^1I3$). Subsequently, two hydrogen atoms transfer from the metal Ir atom to the C atom to form two new C–H bonds ($^1I3 \rightarrow {}^1TS3 \rightarrow {}^1I4 \rightarrow {}^1TS4 \rightarrow {}^1I5$). The H atom of the $CH_2$ moiety is activated and transferred to the Ir metal ($^1I5 \rightarrow {}^1TS5 \rightarrow {}^1I6$); then, the H atom migrates from the Ir metal to the C atom which is not coordinated to other H atoms ($^1I6 \rightarrow {}^1TS6 \rightarrow {}^1I7$). After the CC bond is cleft, the intermediate $^2I8$ is formed, which involves two equivalent $C_2H_2$ moieties—either one can be liberated to form

the final product ***P1*** ($^3IrC_2H_2^+/C_2H_2$). For the pathway for the generation of $IrC_4H_2^+/H_2$, there is the rearrangement steps from $^1I3$ to form intermediate $^1I10$ ($^1I3 \rightarrow {}^1TS8 \rightarrow {}^1I9 \rightarrow {}^1TS9 \rightarrow {}^1I10$). The final product $^1IrC_4H_2^+$ is generated with the liberation of $H_2$. Another possible pathway is given in Figure S4.

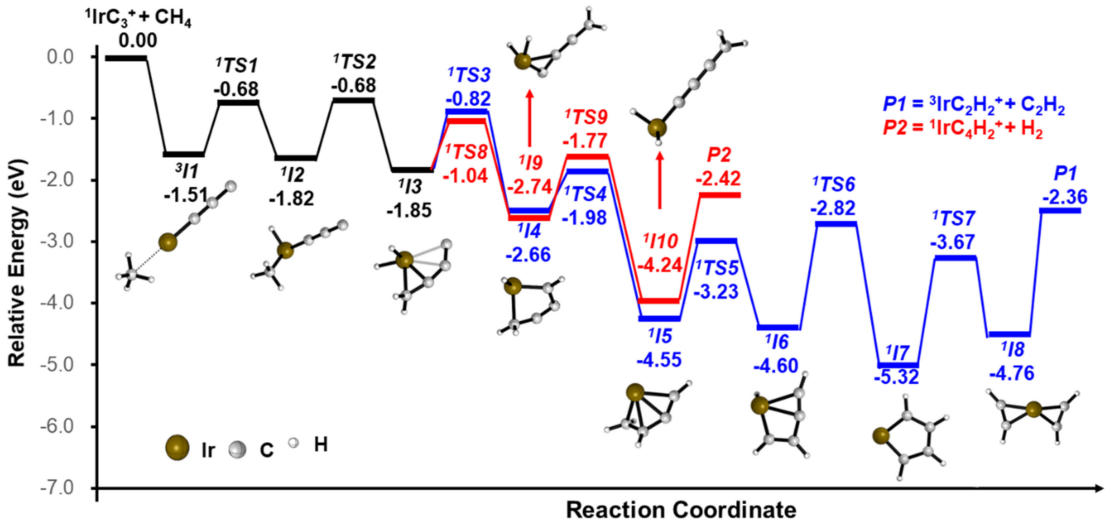


**Figure 2.** Reaction pathways for generating $IrC_2H_2^+/C_2H_2$ (blue trace) and $IrC_4H_2^+/H_2$ (red trace) from the reaction of $IrC_3^+$ and $CH_4$, calculated at the BMK level. The zero-point vibrational energy-corrected energies (in eV) relative to the entrance channel are given.

The pathways for the $PtC_3^+ + CH_4$ reaction are shown in Figure 3. Details and other possible pathways are given in Figures S5–S7. The reaction pathway starts from the encounter complex $^2I1$, followed by the formation of a stable intermediate $^2I2$ via the approaching of $CH_4$ to the terminal carbon of $PtC_3^+$ ($^2I1 \rightarrow {}^2TS1 \rightarrow {}^2I2$), where the first C–H activation takes place. The $CH_3$ moiety of $^2I2$ is transferred to form $^2I3$, where $CH_3$ is loosely coordinated to $PtC_3H^+$. The final product *P1* (−0.46 eV) is generated with the liberation of $CH_3$. The energy of *P1* is higher than the transition states from $^2I2$ to *P2*/*P3*, which can explain the weak peak of $PtCH_3^+$, compared with $PtC_4H_2^+$ and $PtC_2H_2^+$. From $^2I2$, the H atom from the $CH_3$ moiety is activated and transferred to the metal center to form intermediate $^2I4$ ($^2I2 \rightarrow {}^2TS3 \rightarrow {}^2I4$). The H atom subsequently migrates from the Pt metal to the terminal C atom to form intermediate $^2$I5 ($^2I4 \rightarrow {}^2TS4 \rightarrow {}^2I5$). After rearrangement ($^2I5 \rightarrow {}^2TS5 \rightarrow {}^2I6$), the H atom of the $CH_2$ moiety is activated and transferred to the Pt metal again ($^2I6 \rightarrow {}^2TS6 \rightarrow {}^2I7$). Then, the H atom migrates from the Pt metal to C atom which is not coordinated to other H atoms ($^2I7 \rightarrow {}^2TS7 \rightarrow {}^2I8$). After the C and Pt atoms are bonded, the stable intermediate $^2I9$ with a five-membered ring is generated. After the CC bond is cleft, the intermediate $^2I10$ is formed, which involves two equivalent $C_2H_2$ moieties—either one can be liberated to form the final product *P2* ($^2PtC_2H_2^+/C_2H_2$). For another pathway to generate $PtC_4H_2^+/H_2$, after the rearrangement from $^2I5$ to form $^2I11$, the H atom of the $CH_2$ moiety is activated and transferred to the Pt metal again ($^2I11 \rightarrow {}^2TS11 \rightarrow {}^2I12$). The subsequent reaction pathway is the H–H bond formation; then, the final product $PtC_4H_2^+$ is generated with the liberation of $H_2$.

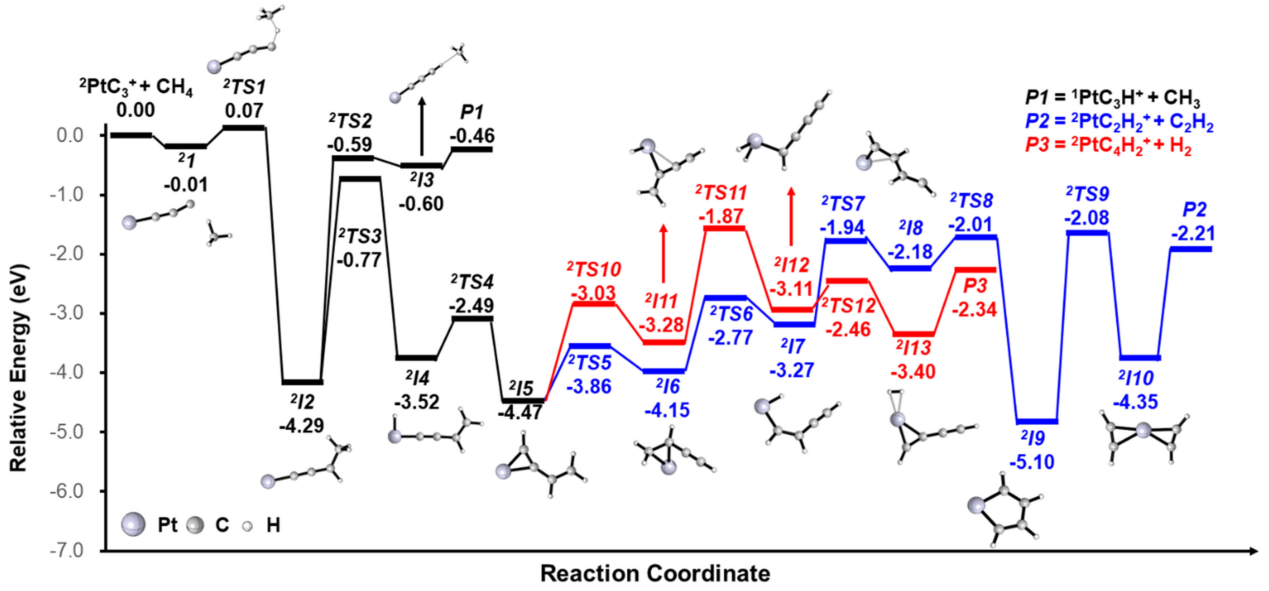


**Figure 3.** Reaction pathways for generating $PtC_2H_2^+/C_2H_2$ (blue trace), $PtC_4H_2^+/H_2$ (red trace) and $PtC_3H^+/CH_3$ from the reaction of $PtC_3^+$ and $CH_4$, calculated at the BMK level. The zero-point vibrational energy-corrected energies (in eV) relative to the entrance channel are given.

For the reactions of the $IrC_3^+$ and $PtC_3^+$ with $CH_4$, we could find the hydrogen abstraction reaction products $PtC_3H^+$ and no $IrC_3H^+$ was observed. Based on our calculations, the reactive sites play a key role. There are two possible sites, the metal and terminal carbon atom (the other two carbon atoms are fully bonded). For $IrC_3^+/CH_4$, the barrier to the first C–H activation on the terminal C atom (+0.04 eV; see Figure S4) is higher in energy than $^1TS1$ (−0.68 eV). Based on the lack of $IrC_3H^+$ observed, we confirm that the reactive site of the first C–H activation is the Ir atom. For $PtC_3^+/CH_4$, the energy required for the first C–H bond activation on Pt and C atoms is +0.01 ($^2TSX3$) and +0.07 eV ($^2TS1$), given in Figure 3 and Figure S6, respectively. Though the Pt atom, as a reactive site, is favorable, the transition state of H atom transfer as the next step (+0.19 eV, $^2TSX4$; Figure S4) is higher in energy than $^2TS1$. Based on the observation of $PtC_3H^+$ in the experiment, we confirm that the terminal carbon atom can be a reactive site for $PtC_3^+/CH_4$.

As we all know, metals have a stronger adsorption capacity for methane than non-metals. The different reactive sites can be explained by the analysis of the orbital. In the $PtC_3^+$ species, platinum uses two of the six valence orbitals (s and d) to form a σ- and π-bond with the adjacent carbon atom. This leaves seven electrons occupying the four remaining non-bonding orbitals on platinum, such that there are no empty orbitals on the metal. Therefore, it is hard for the C−H bond to donate electron density to the metal and the energy of the transition state $^2TSX3$ is a little higher than the $^2TS1$ in Figure 3. For the $IrC_3^+$ species, Ir uses two of the six valence orbitals (s and d) to form a bond with the adjacent carbon atom, which leaves six electrons occupying the four remaining non-bonding orbitals on the Ir atom, such that there are enough empty orbitals on the metal, which is beneficial for the C–H bond activation of $CH_4$. This can explain why the barrier to the first C–H activation on the terminal C atom (+0.04 eV) is higher than that of $^1TS1$ (−0.68 eV). Our work demonstrates that the orbitals of the metal influence the selection of the reactive sites for the activation of methane. The different reactive sites result in different reaction channels.

In conclusion, the activation of methane mediated by $MC_3^+$ ($M$ = Ir and Pt) were comparatively studied at room temperature by gas-phase experiments with theoretical calculations. Mass spectrometric studies on the reactions of the $MC_3^+$ ($M$ = Ir and Pt) ions with $CH_4$ show that two main reaction channels were observed. The first channel is the formation of the $MC_2H_2^+$ cation with the release of neutral $C_2H_2$. The second channel is

the generation of the $MC_4H_2^+$ ion with concomitant elimination of a dihydrogen molecule. Besides that, $PtC_3H^+$ could be found in the experiments, while $IrC_3H^+$ could not. Quantum chemical calculations suggest that the $MC_3^+$ ($M$ = Ir and Pt) ions have a linear $M$-C-C-C$^+$ structure. The Ir atom is the reactive site for the reaction of $IrC_3^+/CH_4$. The generation of the $PtC_3H^+$ and PESs can confirm that the terminal carbon atom is the reactive site for $PtC_3^+/CH_4$. The orbitals of the metal influence the selection of the reactive sites for methane activation, which results in the different reaction channels. Our work is helpful for understanding reactive sites of methane activation.

**Supplementary Materials:** The following are available online, Figure S1: The optimized geometries of the $[IrC_3]^+$ and $[PtC_3]^+$ isomers at the BMK/def2-TZVP level. The relative energies relative to the global minimum structure (in eV), symmetry and electronic states are shown; Figure S2: The optimized geometries of the $[IrC_2H_2]^+/[PtC_2H_2]^+$ (top), $[IrC_4H_2]^+/[PtC_4H_2]^+$ (middle) and $[IrC_3H]^+/[PtC_3H]^+$ (bottom) isomers at the BMK/def2-TZVP level. The relative energies relative to the global minimum structure (in eV), symmetry and electronic states are shown; Figure S3: The detailed potential energy profiles of the reaction of $IrC_3^+$ and $CH_4$ in Figure 2. The energies are given in eV; Figure S4: The other possible potential energy profiles of the reaction of $IrC_3^+$ and $CH_4$. The energies are given in eV; Figure S5. The detailed potential energy profiles of the reaction of $PtC_3^+$ and $CH_4$ in Figure 3. The energies are given in eV; Calculated geometries and potential energy profiles. This material is available free of charge via the Internet.

**Author Contributions:** Conceptualization, X.W. and H.W.; methodology, X.W. and H.W.; formal analysis, W.L.; data curation, W.L.; writing—original draft preparation, Z.L. and X.W.; writing—review and editing, X.W.; supervision, X.W. All authors have read and agreed to the published version of the manuscript.

**Funding:** Support from the National Natural Science Foundation of China (Grant No. 21603037, 21973016).

**Data Availability Statement:** Not available.

**Acknowledgments:** We gratefully acknowledge the financial support from the National Natural Science Foundation of China (Grant No. 21603037, 21973016).

**Conflicts of Interest:** The authors declare no conflict of interest.

**Sample Availability:** Not available.

## References

1. Choudhary, T.; Aksoylu, E.; Goodman, D.W. Nonoxidative Activation of Methane. *Catal. Rev.* **2003**, *45*, 151–203. [CrossRef]
2. Peter, M.; Marks, T.J. Platinum Metal-Free Catalysts for Selective Soft Oxidative Methane Ethylene Coupling. Scope and Mechanistic Observations. *J. Am. Chem. Soc.* **2015**, *137*, 15234–15240. [CrossRef]
3. Schwarz, H. Chemistry with Methane: Concepts Rather than Recipes. *Angew. Chem. Int. Ed.* **2011**, *50*, 10096–10115. [CrossRef]
4. Fokin, A.A.; Schreiner, P.R. Selective Alkane Transformations via Radicals and Radical Cations: Insights into the Activation Step from Experiment and Theory. *Chem. Rev.* **2002**, *102*, 1551–1594. [CrossRef]
5. Schwarz, H.; Shaik, S.; Li, J. Electronic Effects on Room-Temperature, Gas-Phase C-H Bond Activations by Cluster Oxides and Metal Carbides: The Methane Challenge. *J. Am. Chem. Soc.* **2017**, *139*, 17201–17212. [CrossRef]
6. Li, H.-F.; Jiang, L.-X.; Zhao, Y.-X.; Liu, Q.-Y.; Zhang, T.; He, S.-G. Formation of Acetylene in the Reaction of Methane with Iron Carbide Cluster Anions $FeC_3$—Under High-Temperature Conditions. *Angew. Chem. Int. Ed.* **2018**, *57*, 2662–2666. [CrossRef]
7. Geng, C.; Weiske, T.; Li, J.; Shaik, S.; Schwarz, H. Intrinsic Reactivity of Diatomic 3d Transition-Metal Carbides in the Thermal Activation of Methane: Striking Electronic Structure Effects. *J. Am. Chem. Soc.* **2018**, *141*, 599–610. [CrossRef]
8. Ding, X.-L.; Wu, X.-N.; Zhao, Y.-X.; He, S.-G. C–H Bond Activation by Oxygen-Centered Radicals over Atomic Clusters. *Accounts Chem. Res.* **2011**, *45*, 382–390. [CrossRef]
9. Gong, Y.; Zhou, M.; Andrews, L. Spectroscopic and Theoretical Studies of Transition Metal Oxides and Dioxygen Complexes. *Chem. Rev.* **2009**, *109*, 6765–6808. [CrossRef]
10. Böhme, D.K.; Schwarz, H. Gas-Phase Catalysis by Atomic and Cluster Metal Ions: The Ultimate Single-Site Catalysts. *Angew. Chem. Int. Ed.* **2005**, *44*, 2336–2354. [CrossRef]
11. Zhang, G.; Li, S.; Jiang, Y. Dehydrogenation of Methane by Gas-Phase $Os^+$: A Density Functional Study. *Organometallics* **2003**, *22*, 3820–3830. [CrossRef]
12. Wesendrup, R.; Schröder, D.; Schwarz, H. Catalytic $Pt^+$-Mediated Oxidation of Methane by Molecular Oxygen in the Gas Phase. *Angew. Chem. Int. Ed.* **1994**, *33*, 1174–1176. [CrossRef]

13. Irikura, K.K.; Beauchamp, J.L. Methane oligomerization in the gas phase by third-row transition-metal ions. *J. Am. Chem. Soc.* **1991**, *113*, 2769–2770. [CrossRef]
14. Wang, G.; Chen, M.; Zhou, M. Activation of methane by Rh(0): Evidence for direct insertion of rhodium into the C–H bond at cryogenic temperatures. *Chem. Phys. Lett.* **2005**, *412*, 46–49. [CrossRef]
15. Schröder, D.; Roithová, J. Low-Temperature Activation of Methane: It also Works Without a Transition Metal. *Angew. Chem. Int. Ed.* **2006**, *45*, 5705–5708. [CrossRef]
16. Zhang, X.; Schwarz, H. Thermal Activation of Methane by Diatomic Metal Oxide Radical Cations: $PbO^+$center dot as One of the Missing Pieces. *Chemcatchem* **2010**, *2*, 1391–1394. [CrossRef]
17. Feyel, S.; Döbler, J.; Schröder, D.; Sauer, J.; Schwarz, H. Thermal Activation of Methane by Tetranuclear $[V4O10]^+$. *Angew. Chem. Int. Ed.* **2006**, *45*, 4681–4685. [CrossRef]
18. Zhao, Y.-X.; Wu, X.-N.; Wang, Z.-C.; He, S.-G.; Ding, X.-L. Hydrogen-atom abstraction from methane by stoichiometric early transition metal oxide cluster cations. *Chem. Commun.* **2010**, *46*, 1736–1738. [CrossRef]
19. Li, H.-F.; Li, Z.-Y.; Liu, Q.-Y.; Li, X.-N.; Zhao, Y.-X.; He, S.-G. Methane Activation by Iron-Carbide Cluster Anions $FeC_6^-$. *J. Phys. Chem. Lett.* **2015**, *6*, 2287–2291. [CrossRef]
20. Liu, Q.-Y.; Ma, J.-B.; Li, Z.-Y.; Zhao, C.; Ning, C.; Chen, H.; He, S. Activation of Methane Promoted by Adsorption of CO on $Mo_2C_2$−Cluster Anions. *Angew. Chem. Int. Ed.* **2016**, *55*, 5760–5764. [CrossRef]
21. Li, H.-F.; Zhao, Y.-X.; Yuan, Z.; Liu, Q.-Y.; Li, Z.-Y.; Li, X.-N.; Ning, C.-G.; He, S.-G. Methane Activation by Tantalum Carbide Cluster Anions $Ta_2C_4^-$. *J. Phys. Chem. Lett.* **2017**, *8*, 605–610. [CrossRef]
22. Li, J.; Zhou, S.; Schlangen, M.; Weiske, T.; Schwarz, H. Hidden Hydride Transfer as a Decisive Mechanistic Step in the Reactions of the Unligated Gold Carbide [AuC]+ with Methane under Ambient Conditions. *Angew. Chem. Int. Ed.* **2016**, *55*, 13072–13075. [CrossRef]
23. Geng, C.; Li, J.; Weiske, T.; Schwarz, H. A Reaction-Induced Localization of Spin Density Enables Thermal C–H Bond Activation of Methane by Pristine $FeC4^+$. *Chem.-A Eur. J.* **2019**, *25*, 12940–12945. [CrossRef]
24. Wu, X.-N.; Liu, Z.; Wu, H.; Zhang, D.; Li, W.; Huang, Z.; Wang, G.; Xu, F.; Ding, C.-F.; Zhou, M. Reactions of Transition-Metal Carbyne Cations with Ethylene in the Gas Phase. *J. Phys. Chem. A* **2020**, *124*, 2628–2633. [CrossRef]
25. Li, W.; Wu, X.-N.; Liu, Z.; Wu, H.; Zhang, D.; Ding, X.-L. The C/C Exchange in Activation/Coupling Reaction of Acetylene and Methane Mediated by $Os^+$: A Comparison with $Ir^+$, $Pt^+$ and $Au^+$. *J. Phys. Chem. Lett.* **2020**, *11*. [CrossRef]
26. Frisch, M.J.; Trucks, G.W.; Schlegel, H.B.; Scuseria, G.E.; Robb, M.A.; Cheeseman, J.R.; Scalmani, G.; Barone, V.; Mennucci, G.; Petersson, A.; et al. *Gaussian 09, Revision A.1*; Gaussian, Inc.: Wallingford, CT, USA, 2009.
27. Weigend, F.; Ahlrichs, R. Balanced basis sets of split valence, triple zeta valence and quadruple zeta valence quality for H to Rn: Design and assessment of accuracy. *Phys. Chem. Chem. Phys.* **2005**, *7*, 3297–3305. [CrossRef]
28. Boese, A.D.; Martin, J.M.L. Development of density functionals for thermochemical kinetics. *J. Chem. Phys.* **2004**, *121*, 3405–3416. [CrossRef]
29. Lu, L. Molclus program, Beijing Kein Research Center for Natural Science, China. 2016. Available online: http://www.keinsci.com/research/molclus.html (accessed on 1 September 2021).
30. Peng, C.Y.; Ayala, P.Y.; Schlegel, H.B.; Frisch, M.J. Using redundant internal coordinates to optimize equilibrium geometries and transition states. *J. Comput. Chem.* **1996**, *17*, 49–56. [CrossRef]
31. Fukui, K. The Path of Chemical-Reactions—The IRC Approach. *Acc. Chem. Res.* **1981**, *14*, 363–368. [CrossRef]